Desalination and Water Treatment
www.deswater.com

doi: 10.5004/dwt.2021.27665

235 (2021) 241–250
September

Integrated utilization of *Chlorella vulgaris* as biofuel and dye biosorbent

Rehab A. Abdelghaffar[a,*], Samar A. El-Mekkawi[b,*], Fatma Abdelghaffar[a], Sanaa A. Abo El-Enin[b]

[a]*Dyeing, Printing, and Textile Auxiliaries Department, Textile Industries Research Division, National Research Centre, 35 Elbohuth St., Giza, Egypt, P.O. 12622, Tel. +201149995887; emails: rehababdelghaffar@yahoo.com (R.A. Abdelghaffar), fatma-abdelghaffar@hotmail.com (F. Abdelghaffar)*
[b]*Chemical Engineering and Pilot Plant Department, Engineering Research Division, National Research Centre, 35 Elbohuth St., Giza, Egypt, P.O. 12622, Tel. +201145004287; emails: samarelmekkawi@hotmail.com (S.A. El-Mekkawi), sanaaabdelhalim@gmail.com (S.A. Abo El-Enin)*

Received 15 February 2021; Accepted 27 July 2021

ABSTRACT

Rationalizing natural resource consumption is critical to preserve the ecosystem balance. Wastewater treatment and biofuel production using microalgae are routes for a green environment. *Chlorella vulgaris* contains sufficient oil suitable for biofuel. The de-oiled microalgae (R) and carbonized (C) and activated (A) carbon developed from (R) is examined as biosorbents for removing colors from textile wastewater. The pH effect, kinetics, and adsorption equilibrium isotherms were investigated for batch experiments. Results revealed that *C. vulgaris* contains 12.0% oil content and 55.4% saturated fatty acids that enhance its potentiality for biodiesel production. Dry (R) are suitable as biosorbent for monoazo and basic dyes. (C) and (A) is effective for sulfonated diazo and acid dyes, respectively. These results are substantiated using Fourier-transform infrared spectroscopy, scanning electron microscopy with energy-dispersive X-ray analysis, transmission electron microscopy, and X-ray powder diffraction analyses, illustrating the elements and functional groups of each biosorbent. The kinetic data were best fitted to pseudo-first-order during 30 min and pseudo-second-order during 30–110 min, where adsorption capacity values correlated well with the experimental values. Under experimental conditions, the Langmuir isotherm model was best fitted. The maximum adsorption capacity was 21 mg/g at the initial dye concentration of 50 mg/L.

Keywords: Microalgae; Activated biosorbent; Adsorption; Dye removal; Wastewater treatment

1. Introduction

Industries have shown a significant increase in using synthetic complex organic dyes [1]. The textile industry is one of the earliest globally [2] and the largest consumers of dyestuffs. During the dyeing process, approximately 10.0%–15.0% of the dye does not bind to the fabric and is washed away [3,4]. The enormous amount of wastewater produced by dyeing and printing textiles is a serious issue because it tends to bioaccumulate, threatening aquatic life and humans [5–7]. Moreover, these compounds reduce light penetration into rivers, affecting aquatic flora's photosynthetic activities, which, in turn, are reflected in food availability for aquatic organisms [8].

Textile industries mostly use synthetic organic dyes [1,9]. It is challenging to remove dye from the wastewater because of its stability to light, being non-biodegradable, and being high resistance to oxidation [10,11]. Several approaches have been proposed to overcome this problem through conventional physiochemical handlings, such as foam separation, chemical precipitation [12], membrane filtration [13], and

* Corresponding authors.

coagulation [14]. Nevertheless, their application is restricted because of issues such as a metal precipitate, poor settling, high sludge production, and consumption of high amounts of chemicals [15–18].

Activated carbon is the most popular used adsorbent in wastewater treatment globally [19]. This use has led to the search for locally available and renewable materials with high carbon content, such as sugarcane bagasse [20], rice straw, *Eichhornia crassipes* [3], and banana peel powder [21]. Various microorganisms, such as fungi, bacteria, yeasts, and algae, are used in combination with physicochemical processes to develop cheaper alternatives [22]. Microalgae are the most promising biosorbent in purifying and color removal from wastewater [23,24] because of their high sorption capacity and high binding affinity.

The microalgal cell wall contains fatty acids, proteins, polysaccharides, and carbohydrates, which are critical in the biosorption process because of their functional groups, such as carboxyl, hydroxyl, sulfate, phosphate, and amino groups. These functional groups function as binding sites [25]. Microalgae can be used as-is or after oil extraction because of their high carbon content. The sorption potential of a raw biosorbent depends on the chemical structure of both the dye and biosorbent. Furthermore, chemical treatments, such as carbonization and activation, could be applied to increase the active sites or replace the existing sites with more active ones [26].

In this study, oil is extracted and analyzed to assess its potential value as a biofuel. The residual algal biomass is examined as a biosorbent to treat textile wastewater. The de-oiled microalgae (R), carbonized (C), and activated algal biomass (A) are used as biosorbent for four types of mercantile dyes. The pH on Acid Red 1 dye (AR1) adsorption by (A), kinetics, and adsorption equilibrium isotherms were studied for batch experiments using isotherm models. Finally, Fourier-transform infrared spectroscopy (FTIR), scanning electron microscopy with energy-dispersive X-ray analysis (SEM/EDX), transmission electron microscopy (TEM), X-ray powder diffraction (XRD), and Brunauer–Emmett–Teller (BET) analyses are implemented to interpret the effect of functional groups, particle size, and surface texturing in the adsorption process.

2. Material and methods

2.1. Material

Dry biomass of microalgae *Chlorella vulgaris* was obtained from the Algal Biotechnology Unit, National Research Center, Egypt. Several types of dyes were used to examine the potentiality of microalgae as a biosorbent. The sulfonated diazo dye (Reactive Black 5 (RB5)), acid dye (Acid Red 1 (AR1)), basic dye (Violet 16 (V16)), and monoazo dye (Basic Blue 41 (BB41)) were purchased from Sigma-Aldrich Company (United States). The stock solution of each dye was prepared by dissolving 25 mg dye in a 1,000 mL measuring flask with deionized double distilled water. Fig. 1 shows the molecular structure of the dyes used.

2.2. Algal oil extraction

The dry biomass of *C. vulgaris* was crushed into a fine powder. A measured amount of algal powder was mixed with ethanol as a solvent at a ratio of 1:6 w/v (g/mL). The oil extraction process was done using an ultrasonic probe Model Sonics Vibra-Cell V500, Germany, at room temperature (28°C ± 2°C) for 30 min (15 s on and off). The residue of algal cells was dried at 60°C for 8 h to be used as a raw biosorbent (R).

2.3. Gas chromatography analysis

The extracted oil was methylated to detect the fatty acid composition using gas chromatography (GC). Lipid (200 mg) was dissolved in 25 mL solution 5% HCl in methanol and

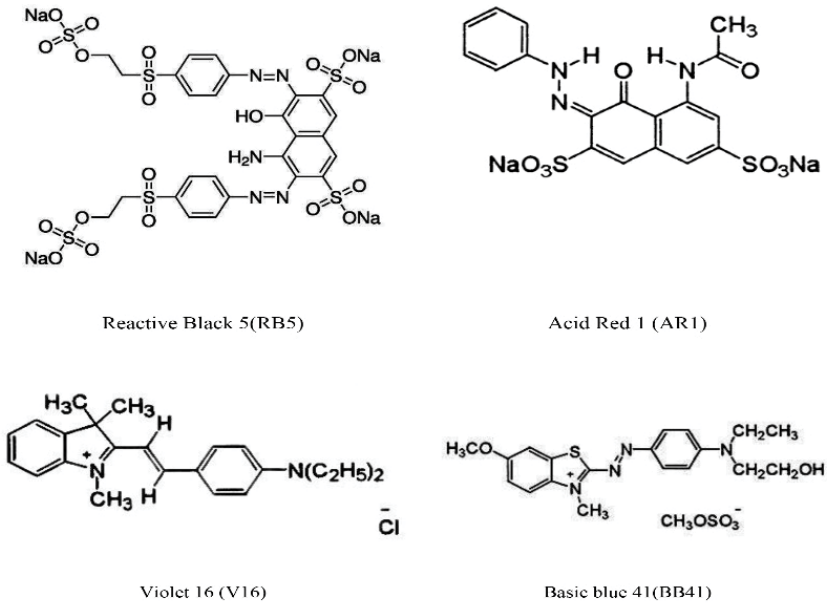

Fig. 1. Molecular structure of dyes.

refluxed for 2 h. The solution was diluted with 25 mL distilled water and extracted with successive portions of diethyl ether in a separating funnel several times. The extracted fatty acid methyl esters were washed several times with distilled water to remove acidity and dried under vacuum at 35°C. The methylation step reduces the oil viscosity to enhance its mobility through the GC column. GC analysis was implemented using the Hewlett-Packard Model 6890 Chromatograph (United States). A flame ionization detector with a split automatic injector and a silica capillary column DB-5 was used. The column dimension is 30 m × 0.25 mm ID with a film thickness of 0.25 μm. Helium was used as a carrier gas at a flow rate of 1 mL/min. The column was maintained at 150°C for 1 min and ramped to 240°C at a rate of 30°C/min, and maintained at 240°C for 30 min.

2.4. Biosorbent preparation

The (C) biosorbent was prepared by burning 50 g of the de-oiled dry algal biomass (R) in a muffle furnace at 400°C for 1 h [1]. The resultant carbonized powder was collected and characterized using FTIR, SEM, XRD, and TEM analyses. The (A) biosorbent was prepared by blending 50 g of (R) biomass with 10 mL of H_2SO_4 (97%) drop-by-drop and stored for 24 h at room temperature (28°C ± 2°C). The excess solution was removed, and the sample was carbonized at 400°C for 1 h in a muffle furnace [1].

2.5. Measurements characterizing the algal biosorbent

2.5.1. FTIR spectroscopy analysis

The functional groups of each (R), (C), and (A) were detected using the FTIR spectrophotometer Model-JASCO FT/IR-4700 (Made in Tokyo, Japan) in the infrared spectral wavelength range of 400 to 4,000 cm^{-1} [27].

2.5.2. Scanning electron microscopy with energy-dispersive X-ray analysis

The algal cells of samples (R), (C), and (A) were morphologically analyzed using SEM (Model, JOEL JAX-480A, China) with an accelerating voltage of 30 kV and magnification between 10.000X and 400.000X to examine the cells' morphology [28]. The SEM was attached to an EDX unit to evaluate the distribution of different elements in the algal biomasses [29].

2.5.3. XRD analysis

The crystallinity of samples (R), (C), and (A) was investigated using the Empyrean diffractometer XRD system (PANalytical, Poland). Diffraction patterns were detected at room temperature (28°C ± 2°C) at an angle (2θ) between 5° and 80° and CuKα radiation (45 kV, 30 mA).

2.5.4. High-resolution TEM

The particle sizes for algal biomass samples (R), (C), and (A) were examined under a high-resolution transmission electron microscope (JEM-1230, JEOL).

2.5.5. Brunauer–Emmett–Teller

The BET analysis technique was volumetric gas adsorption on powder materials to characterize their porous properties and structure. This BET model was based on the adsorption of a monomolecular layer of nitrogen on the sample's surface. The amount of gas adsorbed on the sample surface determines the specific surface area to each 1 g of sample and pour volume [30].

2.6. Adsorption study

The adsorption efficiency as the dye removal percentage was examined for each prepared biosorbent (R), (C), and (A). The experiments were conducted at constant conditions of pH 3 using 0.1 M HCl, at an agitation speed of 400 rpm for 1 h at room temperature (28°C ± 2°C) by adding 2-g biosorbent to 120 mL of the synthetic dye solution of the initial concentration 25 mg/L in a 250 mL conical flask. The concentration of RB5, AR1, BB41, and V16 was determined by measuring the maximum absorbance at 600, 540, 610, and 420 nm, respectively, using the spectrophotometer (UV-1601 Shimadzu, Japan). All adsorption experiments were performed in duplicate, and the average values were reported. The adsorption capacity and the percentage of dye removal (Absorbance %) were calculated using Eqs. (1) and (2), respectively [31].

$$q = \frac{\left(C_0 - C_f\right)V}{X} \tag{1}$$

and

$$\text{Absorbance}\% = \left(\frac{C_0 - C_f}{C_0}\right) \times 100 \tag{2}$$

where C_o and C_f (mg/L) are the initial and final dye concentrations, respectively, q is the amount of dye adsorbed (mg/g), V is the volume of the solution (L), and X is the adsorbed dosage (g/L).

2.7. Effect of pH on dye adsorption

The effect of pH on dye removal was studied using a pH meter Model 350 Jenway (England). The kinetic study was conducted by mixing 2 g (A) with AR1 solution for C_o 32.5 mg/L. The pH of the solution was adjusted to 2, 4, 6, 8, and 10 by adding 0.1 M HCl or 0.1 M NaOH.

2.8. Kinetic study

The adsorption rate is mandatory to obtain the mechanism of the process and the rate-controlling step. Batch kinetic adsorption experiments were conducted in a temperature-controlled stirred system using a 120 mL adsorbate solution. The samples were studied at pH 3, time intervals from 10 to 110 min, and initial dye concentrations of 15, 32.5, and 50 mg/L. The mechanism was analyzed using the pseudo-first-order model [Eq. (3)], pseudo-second-order model [Eq. (4)], and the intraparticle diffusion model [Eq. (5)] [31].

$$\ln\left(q_e - q_t\right) = \ln q_e - k_1 t \tag{3}$$

$$\frac{t}{q_t} = \frac{1}{k_2 q_e^2} + \frac{1}{q_e} t \tag{4}$$

and

$$q_t = k_3 t^{0.5} + C \tag{5}$$

where q_e and q_t are the amount of dye adsorbed (mg/g) at equilibrium and at time t, respectively, k_1 is the rate of first-order adsorption (min^{-1}), k_2 is the rate of second-order sorption (g/mg min), k_3 is the intraparticle diffusion rate constant (mg/(g $min^{0.5}$)), and C is a constant (mg/g).

2.9. Adsorption isotherms

Several adsorption isotherm models were derived to evaluate the adsorption efficiency. The maximum removal was investigated by fitting the adsorption data to Langmuir and Freundlich models.

2.9.1. Langmuir isotherm model

This model describes the monolayer adsorption of adsorbate without migration on the biosorbent's surface. The model's [Eq. (6)] linear form was used to illustrate the equilibrium conditions [32]:

$$\frac{C_e}{q_e} = \frac{1}{bq_m} + \frac{C_e}{q_m} \tag{6}$$

where C_e is the equilibrium concentration (mg/L), q_m is the maximum adsorption capacity (mg/g), and b is the Langmuir constant.

2.9.2. Freundlich isotherm model

This model [Eq. (7)] is used as an empirical model, where K_f and n are the adsorption constants [33].

$$\ln q_e = \ln K_f + \frac{1}{n} \ln C_e \tag{7}$$

3. Results and discussion

3.1. Algal oil extraction

The oil content of *C. vulgaris* is 12%. The ultrasonic probe method is used to increase the recovered lipid because of the cavitation phenomena. The stress from bursting the cavitation bubbles will damage the cell walls of microalgae and release more oil [34]. Furthermore, ethanol is used as a polar solvent to recover a higher oil percentage. The polar solvent accelerates the elimination of the lipid in the cell membrane by decreasing the difference between the surface tensions in the phase boundary [35,36]. The (R) residue is used as a biosorbent, whereas the oil is analyzed to evaluate its potential as a biofuel.

Table 1 shows the GC analysis of the extracted oil. The palmitic acid (C16:0) content is 25.7% and stearic acid (C18:0) content is 21.6%. The saturated fatty acid content is 55.4%, whereas the unsaturated fatty acid content is 41.8%. This profile of fatty acids is suitable for biodiesel production with good quality [37]. The high palmitic percentage improves biodiesel characteristics, such as high oxidation stability, low emissions of NO_x, and high cetane number [38].

3.2. Detecting the most efficient biosorbent

The absorbance results elucidated in Table 2 demonstrate the effectiveness of (R) as a biosorbent for BB41 and V16. However, the results substantiated the need for further processing to increase the absorbance efficiency for RB5 and AR1. These results are achieved by treating 120 mL dye concentration 25 mg/L, adjusted by 0.1 M HCl to pH 3 using 2 g biosorbent agitated at 400 rpm for 1 h at 28°C ± 2°C. Sample (C) has high efficiency as a biosorbent for RB5 and BB41. Because sample (A) is a highly efficient biosorbent for the four types of dyes, it is extremely functional for AR1.

The applied chemical treatment process, either by carbonization or activation, improves the biosorption capacity, alternating the morphological structure of the biosorbent attributed to the difference in chemical structure and functional groups' activity of the dye molecules (Fig. 1).

3.3. Characterizations of de-oiled algal molecular structure biosorbent

3.3.1. FTIR analysis

The spectral FTIR analysis peaks in Fig. 2 show the functional groups of samples (R), (C), and (A). The primary amines (−NH_2) and weak secondary amines (−NH) are elucidated by the peaks ranging from 3,758.58 to 3,830.9 cm^{-1}. These functional groups are basic and rapidly protonated

Table 1
Fatty acid contents of *Chlorella vulgaris* microalgae oil

Fatty acid	Mass fraction %
Lauric acid (C 12:0)	0.7
Myristic acid (C 14:0)	7.4
Palmitic acid (C 16:0)	25.7
Stearic acid (C 18:0)	21.6
Palmitoleic acid (C 16:1)	4.4
Oleic acid (C 18:1)	12.5
Linoleic acid (C 18:2)	5.6
Linolenic acid (C 18:3)	12.3
γ-Linolenic acid (C 18:3n6)	1.7
Arachidonic acid (C20:4)	1.3
Eicosatetraenoic acid (C20:5)	4.0
Saturated fatty acid (SFA)	55.4
Unsaturated fatty acids (USFA)	41.8
Monounsaturated fatty acid (MUSFA)	16.9
Polyunsaturated fatty acid (PUSFA)	24.9
Total fatty acid (TFA)	97.2

Table 2
Absorbance % of each dye using different types of de-oiled algal biomass

Biosorbent type	Absorbance %			
	Reactive Black 5 (RB5)	Acid Red 1 (AR1)	Violet 16 (V16)	Basic Blue 41 (BB41)
(R)	23.55	3.4	82.3	87.9
(C)	95.9	45.9	85.0	97.0
(A)	97.11	98.5	96.45	97.9

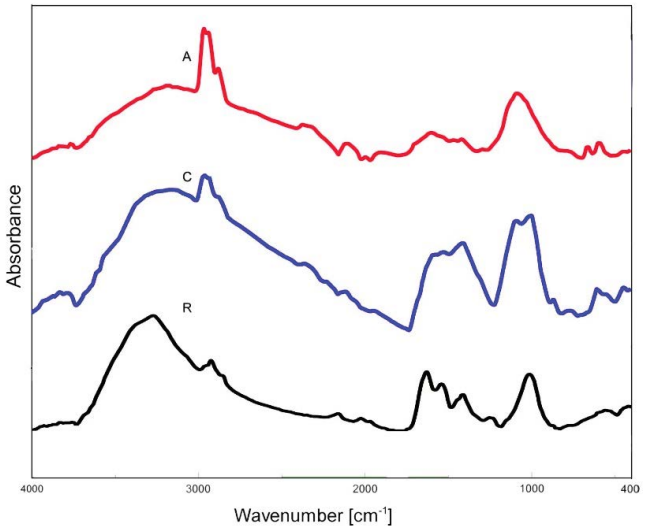

Fig. 2. FTIR bands for (R) biosorbent, (C) carbonized, and (A) activated.

to form ammonium cations [39–41]. The higher intensity peaks for (C) and (A) samples than for (R), explain the higher significant increase in adsorption efficiency for RB5 and AR1 on (C) and (A) than on (R). The adsorption efficiency for RB5 using (C) is increased by 75.4%, whereas the adsorption efficiency for AR1 using (C) is increased by 92.6%.

The border absorption peaks at wavelength 3,156.90 to 3,275.50 cm^{-1} represent the stretching hydroxyl group OH [42,43] that exists in all samples with a high-intensity value for biosorbent (R).

The aliphatic CH_2 group and stretching C–H group is critical in the adsorption process [44]. The peaks at 2,924.52 to 2,965.02 cm^{-1} show the existence of the CH_2 group with asymmetric stretching in the sample (A) more than in (R) and (C). The methyl symmetric stretching C–H group is shown only in the sample (A) at wavelength 2,880.17 cm^{-1}, which is the highest dye removal % for solutions treated with (A).

Sulfur, according to the activation process, appears as an S–H group at wavelength 2,372.01 cm^{-1} for sample (A). The N–O as a symmetric stretching vibration group appears at wavelength 1,542.77 cm^{-1} for sample (R) and 1,529.27 cm^{-1} for sample (C). The nitro group is strongly electron-withdrawing, elucidating the high efficiency of both (R) and (C) as biosorbents for BB41 and V16 according to their ionic structure (Fig. 1). The FTIR-spectrum at 1,094.4 to 1092.48 cm^{-1} represents the Si–O group.

3.3.2. Scanning electron microscopy with energy-dispersive X-ray analysis

Fig. 3 shows the morphological and microstructural changes in the surface of each (R), (C), and (A) algal biomass that was analyzed using SEM. The shape of (R) has a smooth and irregular surface with random heterogeneous sizes. The surfaces of (C) and (A) are regular and have small homogeneous sizes.

The chemical composition of all samples is characterized and examined using EDX analysis (Fig. 3). The most significant result is the increase in carbon w% in (A). The measured carbon w% are 26.05%, 17.69%, and 33.69% for the samples (R), (C), and (A), respectively. The results correlate well with those recorded by FTIR for aliphatic CH_2 and stretching C–H groups. The EDX patterns confirmed the increases in sulfur in (A) because of activation using sulfuric acid.

3.3.3. Transmission electron microscopy

The TEM results show that the particle size of the ground (R) is greater than 200 nm (Fig. 4), whereas the particle size of the (C) sample is in the range of 50–58 nm, and the activation sample (A) is in the range of 12–31 nm. The nanoparticle size of (A) creates a larger surface area, increases the active sites, and allows faster contact between the dye molecules and binding sites [24,45]. These results are integrated with those detected using SEM analysis, where the destruction of the cell membrane, morphology, and homogeneous shape of activated biomass (A) facilitates dye removal.

3.3.4. X-ray powder diffraction

The XRD pattern in Fig. 5 shows the amorphous structure of (R). Some crystalline zones are observed for (C), and a major peak locates at 26.62°. More crystalline zones appear in (A), with a major sharp peak at 25.39°. This result shows the effect of activation on the algae structure that transforms the amorphous structure to crystalline. This crystalline structure with the particle size reduction detected using TEM and the regular homogeneous shape showed using SEM enhances the adsorption capacity [46].

3.3.5. Specific surface area and pore properties

The BET results from Table 3 clarify an increase in the average pore diameter and the total pore volume of samples (C) and (A) compared to (R). The carbonization and activation processes increased the absorption capacity of the surface because of micropore formation. Moreover, the

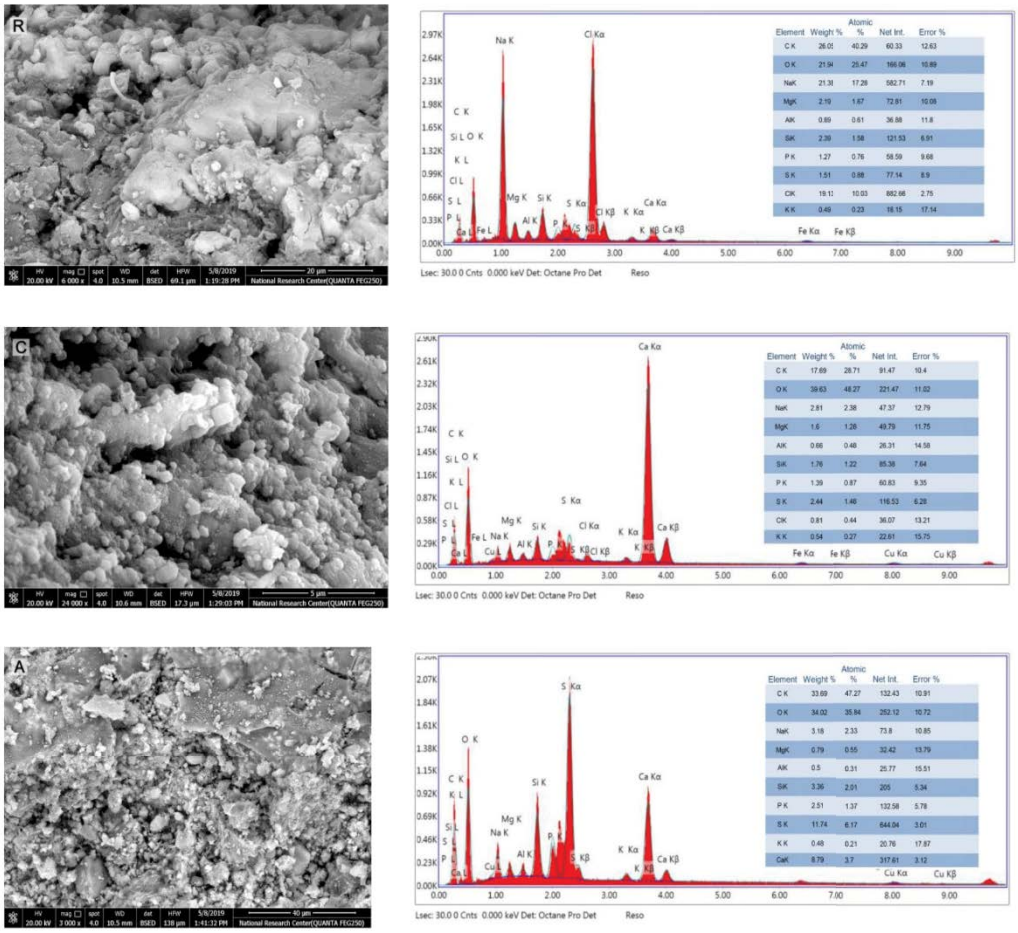

Fig. 3. SEM/EDX images of (R) biosorbent, (C) carbonized, and (A) activated.

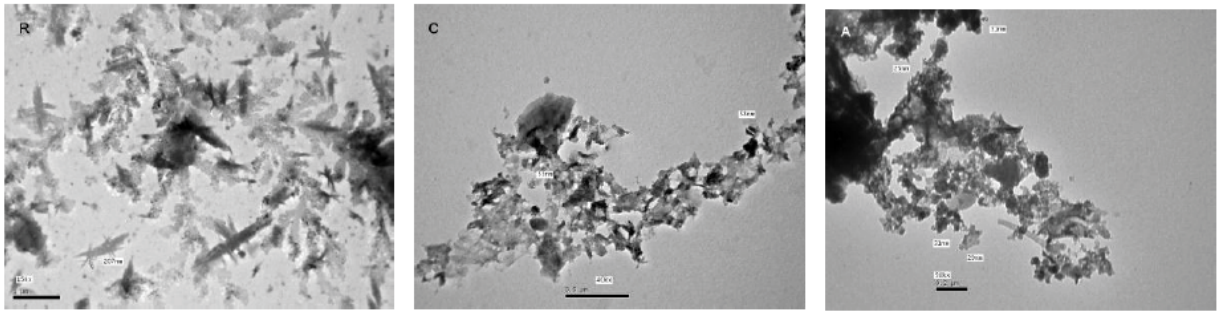

Fig. 4. TEM images of (R) biosorbent, (C) carbonized, and (A) activated.

specific surface area of the sample (R) is larger than that of (C) and (A). The specific surface area from BET measurements classifies the biomass (C) and (A) as nanomaterials, as detected from TEM analysis.

3.4. Effect of pH on AR1 adsorption

The high acidic solution increases the removal percentage more than the alkaline solutions do (Fig. 6). However, the neutral solutions have the lowest removal percentage. Fig. 6 shows the effect of pH on AR1 removal of the initial concentration 32.5 mg/L with a standard deviation range (0.2–0.3). The pH response for the range of initial concentrations (15, 32.5, and 50 mg/L) is the same. Increasing the acidity of the solution increases the positive charge on biosorbent surfaces [47]. Here, the sulfonate groups in AR1 dye enhance the attraction to the functional groups on the biosorbent surface.

3.5. Adsorption kinetics

The dye removal rate is accelerated up to 30 min, then the adsorption rate approaches a plateau (Fig. 7a). The lower initial AR1 concentration results in a higher % removal using

2 g biosorbent, whereas the adsorption capacity increases up to 20 mg/g for 50 mg/L initial dye concentration (Fig. 7b). Fig. 8 shows that the biosorption mechanism obeys the pseudo-first-order model up to 30 min of the adsorption process (Fig. 8a), with the regression coefficient (R^2) approaching 1. The rate coefficient k_1 equals 0.11 min^{-1} for 15 mg/L, and 0.07 min^{-1} for 32.5 and 50 mg/L initial concentrations. After 30 min, the biosorption mechanism follows the pseudo-second-order model (Fig. 8b), with a 0.97 R^2 for all tested initial concentrations. The rate coefficient k_2 equals 0.04 g mg^{-1} min^{-1} for 15 mg/L, 0.02 g mg^{-1} min^{-1} for 32.5 mg/L, and 0.01 g mg^{-1} min^{-1} for 50 mg/L initial concentrations. The intraparticle diffusion model (Fig. 8c) is fitted up to 40 min, with R^2 = 0.93 for both 32.5 and 50 mg/L and R^2 = 0.9 for 15 mg/L initial concentrations. The rate coefficient k_3 equals 1.20 g mg^{-1} min^{-1} for 15 mg/L, 2.35 g mg^{-1} min^{-1} for 32.5 mg/L, and 3.24 g mg^{-1} min^{-1} for 50 mg/L initial concentrations. The linear fitting passes through the origin point. These significances prove that intraparticle diffusion is a rate-limiting step for biosorption processes up to 40 min.

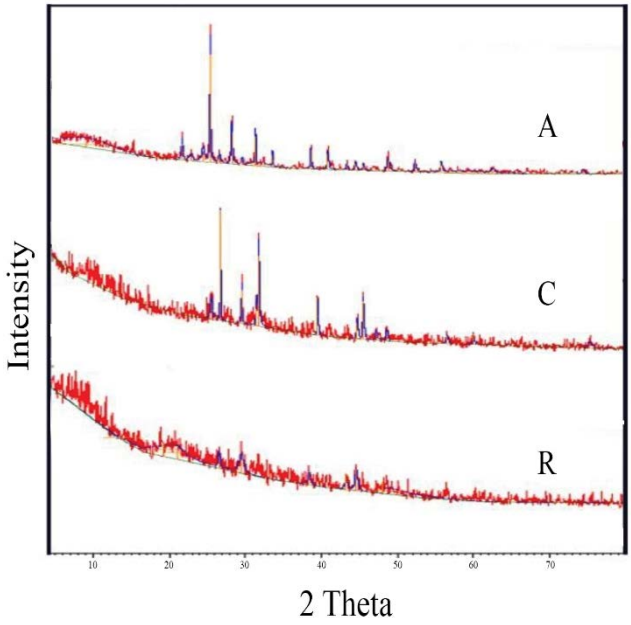

Fig. 5. XRD patterns of (R) biosorbent, (C) carbonized, and (A) activated.

3.6. Adsorption equilibrium

The Langmuir isothermal model is fitted for equilibrium (Fig. 9a) because R^2 = 0.99 for all examined initial AR1 concentrations. The maximum removal q_m is calculated from the Langmuir model plot. It ranges from 7.4 to 21 mg/g for the initial dye concentration range of 15–50 mg/L. The

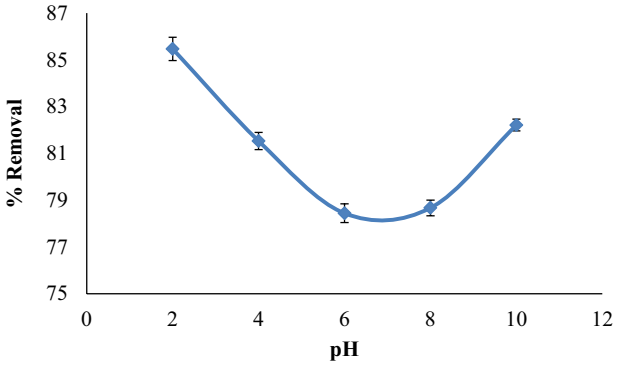

Fig. 6. Effect of pH on AR1 removal at C_o 32.5 mg/L.

Table 3
Results of BET analysis

Absorbent	Specific surface area (m^2/g)	Mean pore diameter (nm)	Total pore volume (cm^3/g)
R	9.0418	5.8915	1.3317
C	1.4855	7.8155	2.9025
A	2.5879	7.6449	4.9460

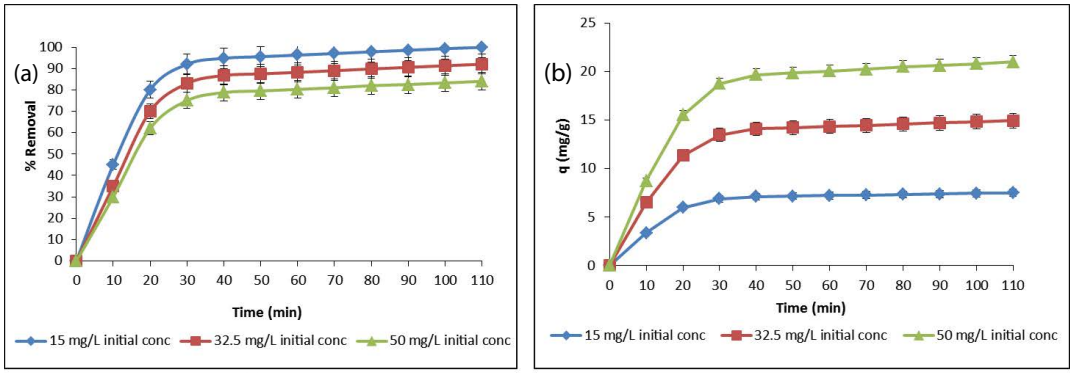

Fig. 7. Effect of initial concentrations and time on (a) removal percent and (b) adsorption capacity at pH 3, 30°C, and 2-g biosorbent.

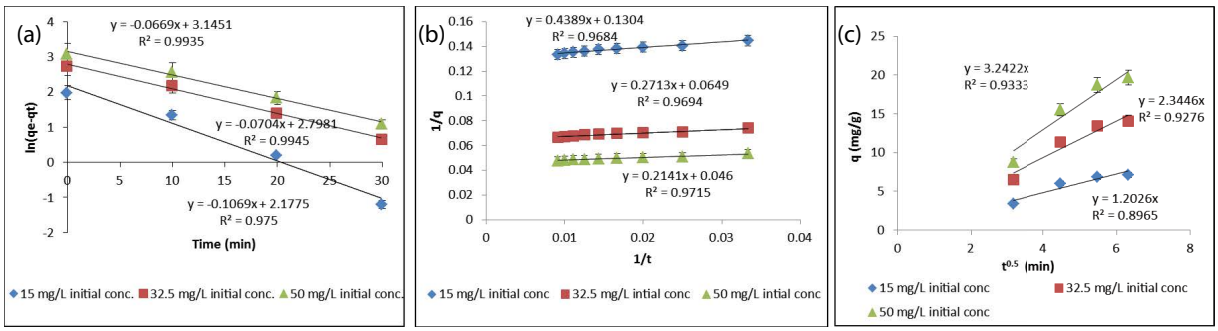

Fig. 8. (a) Pseudo-first-order model for adsorption of AR1 on (A) at pH 3, 30°C, and 2-g biosorbent, contact time up to 30 min. (b) Pseudo-second-order model for adsorption of AR1 on (A) at pH 3, 30°C, and 2-g biosorbent, contact time 30–110 min. (c) Intraparticle diffusion model for adsorption of AR1 on (A) at pH 3, 30°C, and 2-g biosorbent, contact time up to 40 min.

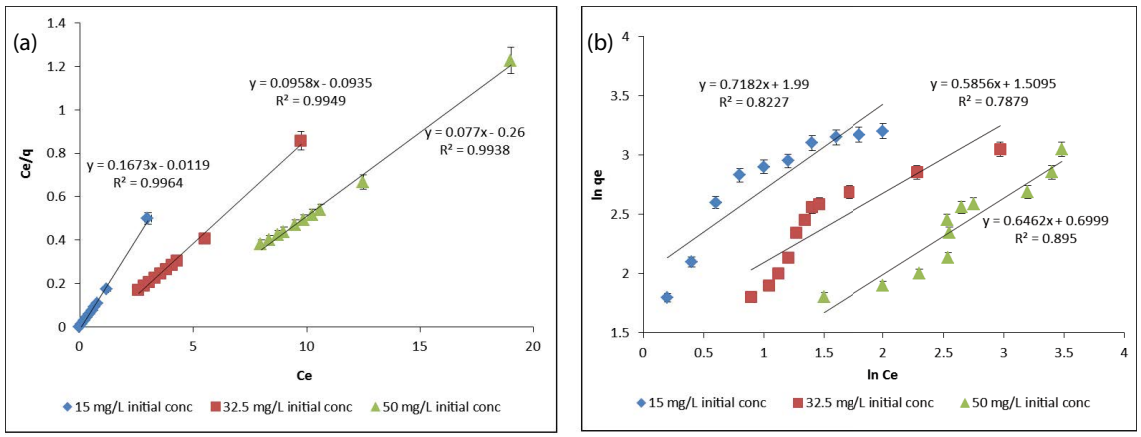

Fig. 9. (a) Langmuir isotherm model for adsorption of AR1 on (A) at pH 3, 30°C, and 2-g biosorbent. (b) Freundlich isotherm model for adsorption of AR1 on (A) at pH 3, 30°C, and 2-g biosorbent.

Freundlich isotherm model is less fitted (Fig. 9b), where the R^2 is 0.8. The adsorption constants K_f corresponds to the adsorption capacity. K_f = 7.32 mg/g for 15 mg/L initial dye concentration, 4.52 mg/g for 32.5 mg/L, and 2.01 mg/g for 50 mg/L. The constant n corresponds to the adsorption intensity and is higher than unity in the range of 1.39–1.71 for the examined dye concentrations.

4. Conclusions

Microalgae have the potential for application in several industries. The extracted fatty acids from *C. vulgaris* are suitable for biodiesel production with good quality. From the biosorbent morphology, after carbonization or activation, the surfaces transform into regular and small homogeneous sizes with a crystalline structure. These treatments increase the surface area with a porous structure, enhancing its adsorption capacity. The nanoparticles obtained have a high surface-to-volume ratio, resulting in increased surface reactivity. This integrated approach of bio-oil extraction and biosorbent production is an environmentally friendly process from natural nonedible resources. The acid dye removal percentage is more affected for acidic solutions at different dye concentrations. The biosorption process up to 30 min obeys the pseudo-first-order model and intraparticle diffusion; after that, it follows the pseudo-second-order model. The equilibrium data fit better with the Langmuir isotherm model than with the Freundlich isotherm model. The maximum adsorption capacity was 21 mg/g at an initial dye concentration of 50 mg/L, pH 3, and 30°C for 40 min.

Acknowledgments

This paper was supported by the National Research Centre in Egypt; we highly appreciate the central laboratories for conducting the tests in this research.

References

[1] M. Alaguprathana, M. Poonkothai, Bioremediation of textile dyeing effluent using algae – a review, J. Adv. Microbiol., 7 (2017) 1–12.
[2] P.H. Nakhate, K.K. Moradiya, H.G. Patil, K.V. Marathe, G.D. Yadav, Case study on sustainability of textile wastewater treatment plant based on lifecycle assessment approach, J. Cleaner Prod., 245 (2020) 118929, doi: 10.1016/j.jclepro.2019.118929.
[3] M.M. El-Zawahry, F. Abdelghaffar, R.A. Abdelghaffar, A.G. Hassabo, Equilibrium and kinetic models on the adsorption of Reactive Black 5 from aqueous solution using *Eichhornia crassipes*/chitosan composite, Carbohydr. Polym., 136 (2016) 507–515.
[4] M. Shahid, Y. Zhou, R.-C. Tang, G. Chen, W.A. Wani, Colourful and antioxidant silk with chlorogenic acid: process

development and optimization by central composite design, Dyes Pigm., 138 (2017) 30–38.
[5] A. Kausar, M. Iqbal, A. Javed, K. Aftab, Zill-i-Huma Nazli, H.N. Bhatti, S. Nouren, Dyes adsorption using clay and modified clay: a review, J. Mol. Liq., 256 (2018) 395–407.
[6] H. Yang, A. Sheikhi, T.G. van De Ven, Reusable green aerogels from cross-linked hairy nanocrystalline cellulose and modified chitosan for dye removal, Langmuir, 32 (2016) 11771–11779.
[7] A.Y.W. Sham, S.M. Notley, Adsorption of organic dyes from aqueous solutions using surfactant exfoliated graphene, J. Environ. Chem. Eng., 6 (2018) 495–504.
[8] Y. Lebron, V. Moreira, L. Santos, Studies on dye biosorption enhancement by chemically modified *Fucus vesiculosus*, *Spirulina maxima* and *Chlorella pyrenoidosa* algae, J. Cleaner Prod., 240 (2019) 118197, doi: 10.1016/j.jclepro.2019.118197.
[9] X. Chen, Q. Deng, S. Lin, C. Du, S. Zhao, Y. Hu, A new approach for risk assessment of aggregate dermal exposure to banned azo dyes in textiles, Regul. Toxicol. Pharmacol., 91 (2017) 173–178.
[10] M.M. El-Zawahry, F. Abdelghaffar, R.A. Abdelghaffar, H.M. Mashaly, Functionalization of the aquatic weed water hyacinth *Eichhornia crassipes* by using zinc oxide nanoparticles for removal of organic dyes effluent, Fibers Polym., 17 (2016) 186–193.
[11] A. Arunachalam, R.G. Chaudhuri, E. Iype, B.P. Kumar, Surface modification of date seeds (*Phoenix dactylifera*) using potassium hydroxide for wastewater treatment to remove azo dye, Water Pract. Technol., 13 (2018) 859–870.
[12] F. Wei, M.J. Shahid, G.S.H. Alnusairi, M. Afzal, A. Khan, M.A. El-Esawi, Z. Abbas, K. Wei, I.E. Zaheer, M. Rizwan, S. Ali, Implementation of floating treatment wetlands for textile wastewater management: a review, Sustainability, 12 (2020) 5801, doi: 10.3390/su12145801.
[13] J. Guo, Q. Zhang, Z. Cai, K. Zhao, Preparation and dye filtration property of electrospun polyhydroxybutyrate–calcium alginate/carbon nanotubes composite nanofibrous filtration membrane, Sep. Purif. Technol., 161 (2016) 69–79.
[14] S. Hussain, N. Amin, S.A. Khan, Quartzite an efficient adsorbent for the removal of anionic and cationic dyes from aqueous solutions, Arabian J. Chem., 13 (2020) 4731–4740.
[15] V. Jegatheesan, B.K. Pramanik, J. Chen, D. Navaratna, C.Y. Chang, L. Shu, Treatment of textile wastewater with membrane bioreactor: a critical review, Bioresour. Technol., 204 (2016) 202–212.
[16] H.R. Rajabi, H. Arjmand, H. Kazemdehdashti, M. Farsi, A comparison investigation on photocatalytic activity performance and adsorption efficiency for the removal of cationic dye: quantum dots vs. magnetic nanoparticles, J. Environ. Chem. Eng., 4 (2016) 2830–2840.
[17] H. Li, S. Wu, C. Du, Y. Zhong, C. Yang, Preparation, performances, and mechanisms of microbial flocculants for wastewater treatment, Int. J. Environ. Res., 17 (2020) 1360, doi: 10.3390/ijerph17041360.
[18] L. Yao, L. Zhang, R. Wang, S. Chou, Z. Dong, A new integrated approach for dye removal from wastewater by polyoxometalates functionalized membranes, J. Hazard. Mater., 301 (2016) 462–470.
[19] A.N. Alene, G.Y. Abate, A.T. Habte, Bioadsorption of basic blue dye from aqueous solution onto raw and modified waste ash as economical alternative bioadsorbent, J. Chem., 2020 (2020) 1–11, doi: 10.1155/2020/8746035.
[20] F. Abdelghaffar, R.A. Abdelghaffar, S.A. Mahmoud, B.M. Youssef, Modified sugarcane bagasse for the removal of anionic dyes from aqueous solution, Pigm. Resin Technol., 48 (2019) 464–471.
[21] L. Zeghoud, M. Gouamid, O.B. Mya, A. Rebiai, M. Saidi, Adsorption of methylene blue dye from aqueous solutions using two different parts of palm tree: palm frond base and palm leaflets, Water Air Soil Pollut., 230 (2019) 195, doi: 10.1007/s11270-019-4255-1.
[22] N.H. Brahmbhatt, R. Jasrai, The role of algae in bioremediation of textile effluent, Int. J. Eng., 4 (2016) 443–453.
[23] S. Elumalai, G. Saravanan, The role of microalgae in textile dye industrial wastewater recycle (phycoremediation), Int. J. Pharm. Biol. Sci., 7 (2016) 662–673.
[24] H. Zohoorian, H. Ahmadzadeh, M. Molazadeh, M. Shourian, S. Lyon, Chapter 41 – Microalgal Bioremediation of Heavy Metals and Dyes, O. Konur, Ed., Handbook of Algal Science, Technology and Medicine, Academic Press, Elsevier, Amsterdam, 2020, pp. 659–674.
[25] A. Maruthanayagam, P. Mani, K. Kaliappan, S. Chinnappan, In vitro and in silico studies on the removal of methyl orange from aqueous solution using *Oedogonium subplagiostomum* AP1, Water Air Soil Pollut., 231 (2020) 232, doi: 10.1007/s11270-020-04585-z.
[26] S. Sharmila, K. Amaraselvam, L. Jeyanthi Rebecca, E. Kowsalya, Biosorption of textile effluent using marine algae, Int. J. Pharm. Sci. Rev. Res., 39 (2016) 108–111.
[27] A. Brangule, R. Šukele, D. Bandere, Herbal medicine characterization perspectives using advanced FTIR sample techniques–diffuse reflectance (DRIFT) and photoacoustic spectroscopy (PAS), Front. Plant Sci., 11 (2020) 356, doi: 10.3389/fpls.2020.00356.
[28] E.A. Ahmed, S. Abo Elenin, H. Mahamoud, Solvent extraction techniques of lipid from algal species in wastewater treatment station, Egypt. J. Chem., 62 (2019) 1551–1562.
[29] M.E. Sastre de Vicente, P. Rodriguez-Barro, R. Herrero, T. Vilariño, P. Lodeiro, J.L. Barriada, Chapter 42 – Biosorption of Chemical Species by *Sargassum* Algal Biomass: Equilibrium Data, O. Konur, Ed., Handbook of Algal Science, Technology and Medicine, Academic Press, 2020, pp. 675–696.
[30] A. Sukoyo, G. Djoyowasito, Y. Wibisono, Unravelling the potency of activated carbon powder derived from cultivated marine microalgae as a promising filler in mixed matrix membranes, AgriEngineering, 1 (2019) 188–204.
[31] I.J. Intidhar, A.C. Luqman, C.S.Y. Thomas, J.B. Siti Nurul Ain, Equilibrium, kinetics and thermodynamic adsorption studies of acid dyes on adsorbent developed from kenaf core fiber, Adsorpt. Sci. Technol., 36 (2018) 1–19, doi: 10.1177/0263617417715532.
[32] K.D. Keno, G. Erastus, M.O. Godfrey, M.M. Eliakim, Kinetic, sorption isotherms, pseudo-first-order model and pseudo-second-order model studies of Cu(II) and Pb(II) using defatted *Moringa oleifera* seed powder, J. Phytopharm., 5 (2016) 71–78.
[33] A. Murcia-Salvador, J.A. Pellicer, M.I. Fortea, V.M. Gómez-López, M.I. Rodríguez-López, E. Núñez-Delicado, J.A. Gabaldón, Adsorption of direct blue 78 using chitosan and cyclodextrins as adsorbents, Polymers, 11 (2019) 1003, doi: 10.3390/polym11061003.
[34] Y.A. Ma, Y.M. Cheng, J.W. Huang, J.F. Jen, Y.S. Huang, C.C. Yu, Effects of ultrasonic and microwave pretreatments on lipid extraction of microalgae, Bioprocess. Biosyst. Eng., 37 (2014) 1543–1549.
[35] R. Tir, P.C. Dutta, A.Y. Badjah Hadj Ahmed, Effect of the extraction solvent polarity on the sesame seeds oil composition, Eur. J. Lipid Sci. Technol., 114 (2012) 1427–1438.
[36] H.S. Basily, M.M. Nassar, G.I. El Diwani, S.A. Abo El-Enin, Extraction of algal lipid as a natural cosmetic component, Egypt. Pharm. J., 17 (2018) 13–20.
[37] M. Jay, M. Kawaroe, H. Effendi, Lipid and fatty acid composition microalgae *Chlorella vulgaris* using photobioreactor and open pond, IOP Conf. Ser.: Earth Environ. Sci., 141 (2018) 012015, doi: 10.1088/1755-1315/141/1/012015.
[38] I.S. Yang, E.S. Salama, J.O. Kim, S.P. Govindwar, M.B. Kurade, M. Lee, B.H. Jeon, Cultivation and harvesting of microalgae in photobioreactor for biodiesel production and simultaneous nutrient removal, Energy Convers. Manage., 117 (2016) 54–62.
[39] A. Silva, R.N. Coimbra, C. Escapa, S.A. Figueiredo, O.M. Freitas, M. Otero, Green microalgae *Scenedesmus obliquus* utilization for the adsorptive removal of nonsteroidal anti-inflammatory drugs (NSAIDs) from water samples, Int. J. Environ. Res., 17 (2020) 3707, doi: 10.3390/ijerph17103707.
[40] M. Déniel, F. Lagarde, A. Caruso, N. Errien, Infrared spectroscopy as a tool to monitor interactions between

nanoplastics and microalgae, Anal. Bioanal. Chem., 412 (2020) 4413–4422.
[41] X.B. Tan, M.K. Lam, Y. Uemura, J.W. Lim, C.Y. Wong, A. Ramli, K.T. Lee, Semi-continuous cultivation of *Chlorella vulgaris* using chicken compost as nutrients source: growth optimization study and fatty acid composition analysis, Energy Convers. Manage., 164 (2018) 363–373.
[42] S. Kumar, A.S. Ahluwalia, M.U. Charaya, Adsorption of orange-G dye by the dried powdered biomass of *Chlorella vulgaris* Beijerinck, Curr. Sci., 116 (2019) 604–611.
[43] V. Kumar, M. Kashyap, S. Gautam, P. Shukla, K.B. Joshi, V. Vinayak, Fast Fourier infrared spectroscopy to characterize the biochemical composition in diatoms, J. Biosci., 43 (2018) 717–729.
[44] M. Asemani, A.R. Rabbani, H. Sarafdokht, Evaluation of oil fingerprints similarity by a novel technique based on FTIR spectroscopy of asphaltenes: modified moving window correlation coefficient technique, Mar. Petrol. Geol., 120 (2020) 104542, doi: 10.1016/j.marpetgeo.2020.104542.
[45] I. Khan, K. Saeed, I. Khan, Nanoparticles: properties, applications and toxicitie, Arabian J. Chem., 12 (2019) 908–931.
[46] R. Chikri, N. Elhadiri, M. Benchanaa, Y. El maguana, Efficiency of sawdust as low-cost adsorbent for dyes removal, J. Chem., 2020 (2020) 1–17, doi: 10.1155/2020/8813420.
[47] A. Chham, H. Khouya, M. Oumam, A. Abourriche, S. Gmouh, M. Iarzek, S. Mansouri, N. Elhammoudi, N. Hanafi, H. Hannache, The use of insoluble mater of Moroccan oil shale for removal of dyes from aqueous solution, Chem. Int., 4 (2018) 67–77.